ANOMALY SEGMENTATION IN COVID-19 CT SCAN IMAGES USING LIGHTWEIGHT CNN

Nilesh Narayanrao Narwade[1*], Dr. M. V. Vaidya[2], Dr. B. S. Shetty[3], Dr. R. S. Bhalekar[4]

Abstract:
Chest Computed Tomography (CT) imaging has become an indispensable tool for staging and managing COVID-19. The current evaluation of COVID-19-associated anomalies relies mainly on visual scoring, a subjective and time-consuming process for clinicians. Therefore, there is a critical need for automated methods to quantify CT imaging anomalies for COVID-19, providing vital assistance to healthcare professionals. In response to this challenge, we present Anam-Net(an innovative Anamorphic depth embedding-based lightweight Convolutional Neural Network (CNN)) specialized specifically for the segmentation of anomalies in COVID-19 chest CT images. The important factor in these images, COVID-19 may be seen as ground-glass opacities in the lung region, which represent a threat to significant difficulties for manual segmentation. Anam-Net addresses this complexity by providing an efficient and accurate automated method for identifying and delineating these opacities, thereby aiding in diagnosis and treatment decisions. Anam-Net stands out for its lightweight design, displaying 7.8 times fewer parameters than cutting-edge UNet and its variations. This makes it well-suited for inference on mobile or resource-constrained platforms, including point-of-care devices, without compromising performance. Our extensive experiments with chest CT images demonstrate that Anam-Net achieves commendable For both diseased and normal lung areas, dice similarity scores, reaffirming its efficacy in COVID-19 anomaly segmentation.

[1*]Information Technology, S.G.G.S.I.E. & T., Nanded, Maharashtra, India Nanded, Maharashtra, India nileshnarwade03@gmail.com
[2]Information Technology, S.G.G.S.I.E. & T., Nanded, Maharashtra, India Nanded, Maharashtra, India mvvaidya@sggs.ac.in
[3]Information Technology, S.G.G.S.I.E. & T., Nanded, Maharashtra, India Nanded, Maharashtra, India bsshetty@sggs.ac.in
[4]Physics and General science, S.G.G.S.I.E. & T., Nanded, Maharashtra, India Nanded, Maharashtra, India rsbhalekar@sggs.ac.in

***Corresponding Author:** Nilesh Narayanrao Narwade
*Information Technology, S.G.G.S.I.E. & T., Nanded, Maharashtra, India Nanded, Maharashtra, India nileshnarwade03@gmail.com

DOI: 10.48047/ecb/2023.12.si10.00315

I. Introduction:

Studies have shown that chest CT analysis uses RT-PCR to detect COVID-19[1],[2] with a sensitivity of 0.97, specificity of 0.25, and accuracy of 0.68 [3]. Related findings have been reported elsewhere, indicating the potential of radiological imaging in supporting early COVID-19 screening [5], [6].

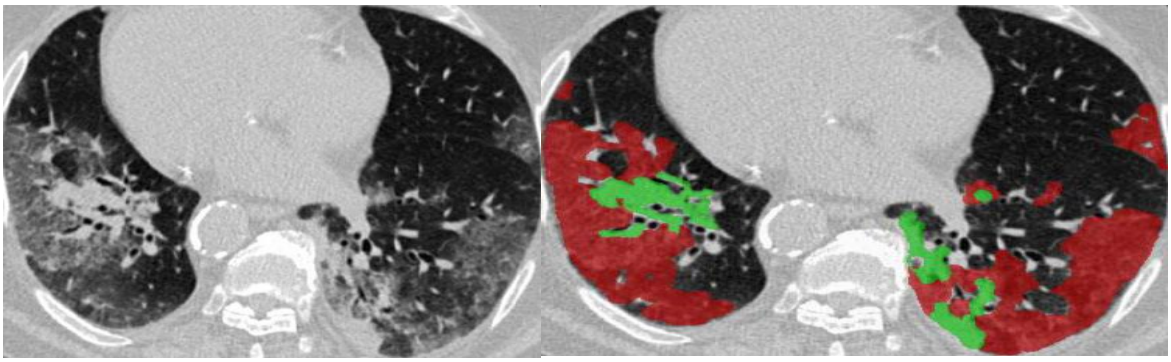

FIGURE 1: Illustration of COVID-19 Lung Infection Regions in CT Axial Slice (A) shows an illustration of COVID-19 infected regions in a CT axial slice. Ground-glass opacity (GGO) and consolidation, respectively, are represented by the red and green masks (B). These pictures were gathered from the cited source [7].

Due to its ability to provide a three-dimensional view of the lung and the ability to observe typical infection signs in CT slices, such as ground-glass opacity (GGO) in the early stage and pulmonary consolidation in the late stage, CT screening is by far the most popular radiological imaging modality [3], [8]. In the fight against COVID-19, qualitative analysis of infections and longitudinal alterations in CT slices can be very useful. However, manually identifying lung infections on CT scans is a taxing and time-consuming task that is frequently influenced by radiologists' clinical experiences and personal biases.

To detect COVID-19 in radiological imaging, deep learning methods have recently been developed [4], [10]. To identify COVID-19 instances from chest radiography pictures, for example, COVID-Net was developed [11]. Radiologists used an anomaly detection model to analyze a large number of chest X-ray images [12]. A location-attention-oriented model was used in CT imaging to estimate the likelihood of COVID-19 infection [13], and a software system based on weakly supervised deep learning using 3D CT volumes was created for COVID-19 detection [14]. Only a few studies have focused on infection segmentation in CT slices, even though many AI systems help diagnose COVID-19 in clinical settings [15], [16]. Several difficulties are addressed in the COVID-19 infection detection on CT slices: (1) The diagnosis of infections is hampered by their high variability in texture, size, and location, especially for minor or insignificant consolidations that may result in false-negative findings in entire CT slices. (2) GGO boundaries have poor contrast and fuzzy appearances, making it difficult to distinguish between them. Inter-class variance is modest. (3) Due to the COVID-19 situation's urgency, it is difficult to gather enough labeled data for training deep models because it takes a lot of resources to obtain high-quality pixel-level annotation of lung infections on CT slices.

Only one public COVID-19 imaging dataset has segmentation labels, despite the fact that many of them concentrate on diagnosis [17]. In this study, we propose a novel COVID-19 Lung Infection Segmentation Deep Network (Inf-Net) to address the difficulties of COVID-19 infection segmentation in CT slices. Our approach uses edge constraint guidance and reverses attention to improve boundary identification after identifying coarse areas of infection. To enhance learning capabilities using a small number of labeled data and propagating information to unlabeled data, we also present a semi-supervised segmentation approach. On the recently created COVID-SemiSeg dataset, we assess the performance of Inf-Net and Semi-Inf-Net, exhibiting superior results compared to leading-edge segmentation models, and furthering the state-of-the-art in COVID-19 lung infection segmentation.

We suggest a novel COVID-19 Lung Infection Segmentation Deep Network (Inf-Net) in this study that is designed especially for CT slices. Our strategy is modeled after the clinical workflow, in which doctors first determine the general location of an infected area and then determine its shape using local indications. We claim that normal tissues can be distinguished from infections by two crucial characteristics: the area and the

boundary. The coarse areas of the COVID-19 infection images are predicted by our Inf-Net initially. Then, it employs edge constraint guidance and reverses attention to implicitly model the borders of these regions. This improves the model's capacity for boundary detection.

We provide a semi-supervised segmentation method that makes use of a small number of labeled images to overcome the issue of limited labeled data. To increase the model's capacity for learning, the system additionally utilizes unlabeled photos. To be more precise, the system propagates unlabeled photos chosen at random through the model. As a result, the performance is superior to certain cutting-edge models. Our three contributions to this study are as follows:

We introduce the cutting-edge CT slice COVID-19 Lung Infection Segmentation Deep Network (Inf-Net). The combined feature, which incorporates contextual information and produces a global map as the first area of guidance for subsequent steps, is created by using a parallel partial decoder (PPD) to aggregate features from high-level layers. Additionally, to create a strong connection between regions and boundary signals, we make use of a collection of implicitly recurring reverse attention (RA) modules and explicit edge-attention direction.

We introduce a semi-supervised segmented technique for segmenting the COVID-19 infection, which effectively mitigates the scarcity of labeled data. Our semi-supervised approach, based on randomly selected propagation, significantly enhances the model's learning ability (refer to § IV for details).
We compile 1600 unidentified pictures from the COVID-19 CT Collection dataset [9] and 100 labeled CT slices from the COVID-19 CT Segmentation dataset to create the semi-supervised COVID-19 infection segmentation dataset (COVID-19 SemiSeg). We demonstrate the superiority of our proposed Inf-Net and Semi-Inf-Net over the majority of cutting-edge segmentation models through thorough experimentation on this dataset, pushing the state-of-the-art performance.

The code and the dataset for our research have been made publicly available at the following repositories:
"https://github.com/DengPingFan/Inf-Net". Our work contributes to the field of COVID-19 lung infection segmentation, providing promising results and potential avenues for future research and development.

II. METHODS

The design of Anam-Net and the suggested method for segmenting anomalies in COVID-19 chest CT images are as follows. Here are the specifics of each of these steps:

A. Extraction of the Lungs:

Extraction of the lung region is the first step in segmenting anomalies in chest CT scans. The procedure outlined in [24] was utilized to obtain the lung masks used in datasets I and II (see Table I). These lung masks were made easily accessible and widely available. A pretrained U-Net architecture with batch normalization was used for the extraction process [33]. A database of 5300 instances was used to train this architecture on 231 examples. Comparing the U-Net (R231) technique to other trained models, including the chest imaging platform (CIP) [24] and progressive holistically nested networks (P-HNNs) [24], it was shown that the U-Net (R231) method was more accurate in segmenting the lungs. The lung pathologies and organizational patterns represented in the training samples for U-Net (R231) included fibrosis, trauma, and other pathologies. This made it possible to accurately separate the lungs from chest CT scans of COVID-19 patients. It is interesting that any method, even straightforward windowing, is determined to be appropriate for the proposed research.

B. Deep Learning to Segment Medical Images:

In recent times, medical image segmentation has seen advancements using various approaches including cross-modality adaptation, knowledge distillation, and neural architectural search (NAS). Some studies have proposed NAS strategies for biomedical segmentation, leveraging macrolevel and microlevel operations for accurate organ segmentation during radiotherapy treatment planning. However, the computational complexity of NAS makes it less suitable for the COVID-19 segmentation task, which demands efficiency due to large training times.

To address the scarcity of labeled data, semisupervised systems have been proposed, combining supervised and regularized components for labeled and unlabeled data, respectively. Unsupervised strategies based on topological loss and knowledge transfer from heavy models through model pruning have also been explored.

User-in-the-loop strategies have been deployed for 2-D and 3-D segmentation of fetal MRI and brain tumors, incorporating user interactions as hard constraints into back propagatable conditional random fields for end-to-end training. Context encoding networks and cross-modality adaptation modules have been introduced to enhance 2-D medical image segmentation between MR and CT images.

Among existing architectures, UNet, SegNet, DeepLabV3+, ResUNet++, UNet++, Attention UNet, and DoubleU-Net exhibit heavy models with specialized computing requirements. In contrast, the ENet architecture offers an efficient solution, designed for the segmentation of semantics in computer vision. ENet's engineered design features bottleneck layers, dilated convolutions, and asymmetric convolutions, enabling it to work with fewer parameters and achieve efficient segmentation. The ENet design consists of a large encoder and a tiny decoder, where the shallow decoder performs upsampling while the deep encoder works on images of lower resolution. Similarly, LEDNet presents another lightweight architecture, employing an encoder-decoder module that uses ResNet as its foundation. The accuracy and speed of segmentation are further improved with the addition of channel-wise split and shuffle operations.

In summary, various deep learning approaches have been applied to medical image segmentation, with ENet and LEDNet emerging as efficient and promising architectures for robust segmentation tasks, including COVID-19 chest CT image analysis.

C. COVID-19 Anomalies Proposed Approach for Segmenting:

The advantages of the symmetric encoder-decoder design of UNet and the efficiency with fewer parameters of ENet are combined in our suggested Anam-Net architecture. To do this, we integrate a novel AD block into a minisymmetric encoder-decoder segmentation module (inspired by [31]).

A 1 × 1 convolution for depthwise compression is used to build the AD-block, which is then followed by a 3 × 3 convolution and a final 1 × 1 convolution for depthwise stretching (further information may be found in Table II). The fundamental idea behind the AD-block is to project or compress the depth-wise dimension of the feature space before performing computationally intensive 3 × 3 convolutions. This low-dimensional embedding with a 1 × 1 projection effectively preserves key details about a sizable input patch [26]. Local feature extraction is then carried out using 3 × 3 convolutions without diminishing the depthwise feature space dimension after this low-dimensional projection. Finally, another 1 × 1 projection stretches the depthwise feature space dimension back to its initial state.

By incorporating the AD-block within our Anam-Net architecture, we ensure effective utilization of feature space and computational resources while maintaining accuracy in segmenting COVID-19 anomalies in chest CT images. This novel approach facilitates precise local feature extraction and efficient depthwise processing, making Anam-Net an efficient and robust solution for COVID-19 anomaly segmentation.

To enable conspicuous and robust feature learning, the proposed Anam-Net architecture has a total of six AD-blocks, three of which are found in the encoder and three of which are found in the decoder. Rectified Linear Unit (ReLU) activation [28], batch normalization [33], and convolution operation are the steps that each convolution layer in Anam-Net takes after each other.

For a comprehensive overview a module for the encoder-decoder and AD-block specifications. These tables provide detailed information about the specific layers and operations used in the Anam-Net architecture, ensuring transparency and clarity in understanding the design and functionality of the proposed model.

Our architecture was then used to split each pixel of unseen test samples into three different categories: background, abnormal-lung region, and normal-lung region. This was done after undergoing end-to-end training. The model produces a probabilistic map with the same spatial dimensions as the input and three distinct maps, one for each category (background, abnormal, and normal).

We calculated the maximum probabilistic score across the three categories for each pixel to give labels to specific pixels. The pixel was assigned to one of the three categories following this score. A noteworthy finding was the identification of the background (non-lung region), as described in Section II-A, ensuring accurate segmentation and delineation of lung abnormalities in the COVID-19 chest CT images during our research.

III. EXPERIMENTS AND IMPLEMENTATION

In this study, we carried out three tests to evaluate the performance of the discussed models using various datasets. A summary of the datasets utilized is presented in Table III, and the details of the experiments are as follows:

Experiment 1: For this study, we used 929 axial chest CT scans from around 49 COVID-19 patients that were made available for public viewing by Radiopedia [30] and the Italian Society of Medical and Interventional Radiology [29].

TABLE I: An Overview Of The Datasets Used In This Study

Dataset No.	Reference	Patients	Total Slices
I	[24]	>40	100
II	[24]	9	829
III	[27]	20	3410

The data was divided into two sets: Data Set I and Data Set II. Data set I, consisting of 100 slices from >40 patients, was utilized for training, with 90 slices chosen for this purpose. We augmented the training data by performing horizontal and vertical flips, resulting in a training set of 270 samples. Data set II, comprising 829 slices from nine patient CT volumes, was used exclusively for testing, with 704 slices selected for this purpose. All images in both datasets were annotated for abnormalities, and masks for ground-glass opacities (GGO), consolidations, and pleural effusion were provided. A single anomalous mask was created using all of these annotations combined. All 704 chest CT images taken into account in this experiment, including dice similarity scores for the anomalous region and inference analysis on resource-constrained platforms, were shown and averaged (see Tables V, VI, and VII).

Experiment 2: We used a collection of 3410 axial chest CT images from 20 COVID-19 patients in this investigation (Data set III in Table I). There are four equal folds in the dataset: F1, F2, F3, and F4. Explicit testing was conducted using fold F4, which contains 545 CT images, and the deep models were trained using threefold cross-validation on folds F1, F2, and F3. Table V shows the averaged merit scores for the three cross folds across all 545 chest CT images used in this experiment.

Experiment 3: In this cross-data set study, the models created in Experiment 2 were tested using the test cases from Experiment 1. This evaluation's goal was to ascertain how successfully the deep models could be used in practical application scenarios. The average merit ratings for the 704 chest CT scans used in this trial are shown in Table VI.

These experiments enabled us to thoroughly assess the performance and generalization capabilities of the proposed Anam-Net architecture and other deep models in segmenting COVID-19 anomalies, providing valuable insights for potential practical applications in medical imaging.

Implementation*:* PyTorch [31] was used to implement the suggested Anam-Net, with a minibatch size of 5. We used the Adam optimizer [32] to optimize the cost function, with an initial learning rate of 5e4 that subsequently decreased by a factor of 0.1 after every 33 epochs. On a Linux workstation with an i9 9900X CPU, 128 GB of RAM, and an NVIDIA Quadro RTX 8000 GPU card, all calculations—including the training of the CNN—were carried out.

We trained cutting-edge techniques including UNet [18], ENet [17], LEDNet [22], UNet++ [19], SegNet [20], Attention UNet [21], and DeepLabV3+ [23] using the same training data and evaluated them using the same test data across all experiments to ensure a fair comparison. We used these practiced models in place of the Anam-Net throughout testing. A brief comparison of each model's parameters, size, typical training time, and inference time is shown in Table IV.

We determined figures of merit, such as specificity, accuracy, sensitivity, and the Dice

TABLE II: Comparative Analysis of Deep Learning Models Used For COVID-19 Anomaly Segmentation. Four crucial factors were compared: the number of training parameters, the size of the model, the training time (for 100 epochs in exp. 1), and the inference time.

Model	Parameters	Model Size	Training time	Inference time
UNet	31.07M	118.24MB	51min	531 ms
ENet	343.7K	1.33MB	15min	248 ms
UNet ++	9.16M	34.95MB	58min	551 ms
SegNet	29.44M	112.31MB	37min	528 ms
Attention UNet	34.87M	133.05MB	63min	569 ms
LEDNet	0.91M	3.8MB	16min	298 ms
DeepLabV3 +	54.70M	208.66MB	42min	895 ms
Anam -Net	4.47M	17.21MB	27min	362 ms

score, for both abnormal and normal classes to statistically assess the segmentation performance of all models. The figures of merit are computed within the range of 0 to 1, with a higher value (close to 1) indicating better model performance. This rigorous evaluation approach enabled us to assess and compare the effectiveness of each model in accurately segmenting COVID-19 anomalies in chest CT images.

IV. HARDWARE DEPLOYMENT

For our research, we explored the hardware deployment of the Anam-Net model on two different platforms. The first platform is the Raspberry Pi 4 Model B, it provides enhanced its features with better processor speed, memory size, and networking than its predecessor. We successfully from PyTorch to TensorFlow Lite, and the learned Anam-Net model was transformed. to enable its deployment on the Raspberry Pi. The Tensorflow Lite version significantly reduced inference time, with the Anam-Net performing 23.3 seconds, while the UNet model took 43.3 seconds. Despite the conversion challenges using third-party tools, the Anam-Net showed promising results on this low-cost embedded system.

Next, we deployed the NVIDIA Jetson AGX Xavier developer kit's Anam-Net model, which is a powerful deep-learning model accelerator. Jetson AGX Xavier boasts impressive performance and energy efficiency compared to its predecessor, Jetson TX2. Inference for the Anam-Net model on the Jetson AGX Xavier was completed in 2.9 seconds as opposed to 5.2 seconds for the UNet model. The Jetson AGX Xavier platform was used to train both the Anam-Net and UNet models, with Anam-Net demonstrating a faster training time (1.49 minutes per epoch) than UNet (3.19 minutes). To extend the applicability to mobile platforms, we developed the CovSeg Android Application using the PyTorch Lite version. The application allows segmenting of COVID-19 anomalies on mobile devices. Both the

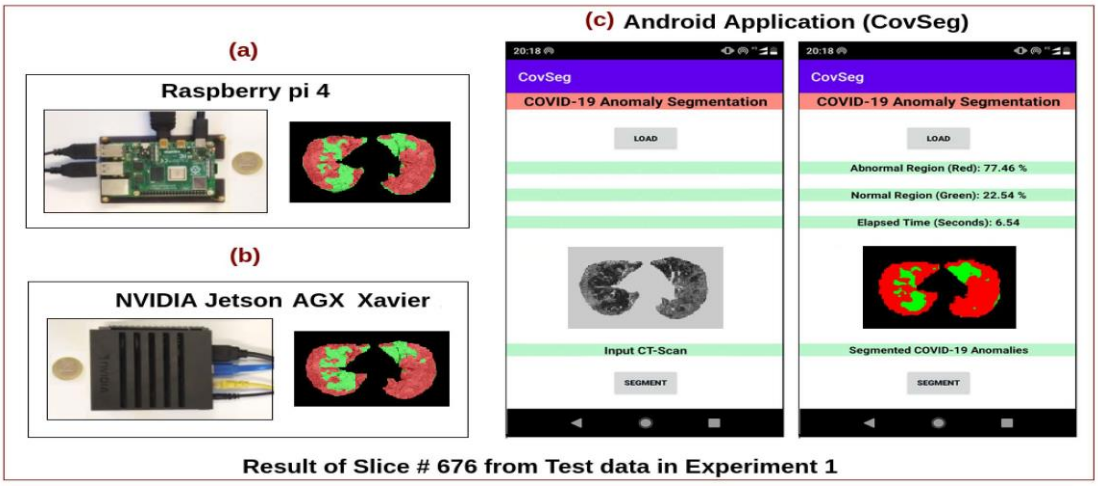

The hardware tools used to deploy the intended COVID-19 abnormalities will be segmented by Anam-Net at the point of care. systems are shown in Figure 2. The part of the lung that is healthy is depicted in green, and the abnormal lung region is depicted in red. Sample Segmented Slice #676 from the Raspberry Pi 4 and experiment 1 test scenarios are shown in Figure (a). The test's

sample segmented slice #676 and the NVIDIA Jetson Xavier scenarios are shown in (b). For form factor comparison, a single Euro coin is shown in these photographs. (c) gives an example slice #676 from the test cases, segmented (Exp. 1) from the Android application (CovSeg) that was developed. The findings of the inference analysis are shown in Table V.

TABLE III: Cost, Memory Space, and Inference Time (in seconds) comparison of the hardware used to deploy the proposed Anam-Net

Device	Inference	Available Memory	Cost
Raspberry Pi 4	Anam -Net:23.3s UNet:43.3s	4GB RAM	$50
NVIDIA Jetson	Anam -Net 2.9s : UNet:5.2s	512-core Volta GPU 32GB RAM	$700
Nokia 5.1Plus	Anam -Net 6.5s UNet:11.3s	3GB RAM	$95

the front and rear ends of the CovSeg application were developed using Android Studio. Inference analysis on a Nokia 5.1 Plus mobile phone demonstrated the successful performance of the Anam-Net model within the application.

Overall, our hardware deployment experiments confirmed the Anam-Net's effectiveness in resource-constrained environments and real-world scenarios, showcasing its potential for point-of-care applications and mobile usage.

V. RESULTS

In the results section, the proposed Anam-Net's performance in segmenting COVID-19 anomalies was evaluated and compared to other models. The method effectively segmented abnormalities in all chest CT images and provided null results when no abnormality was present. Fig. 4 showed example results, and Table VI displayed the Dice scores for the abnormal class.

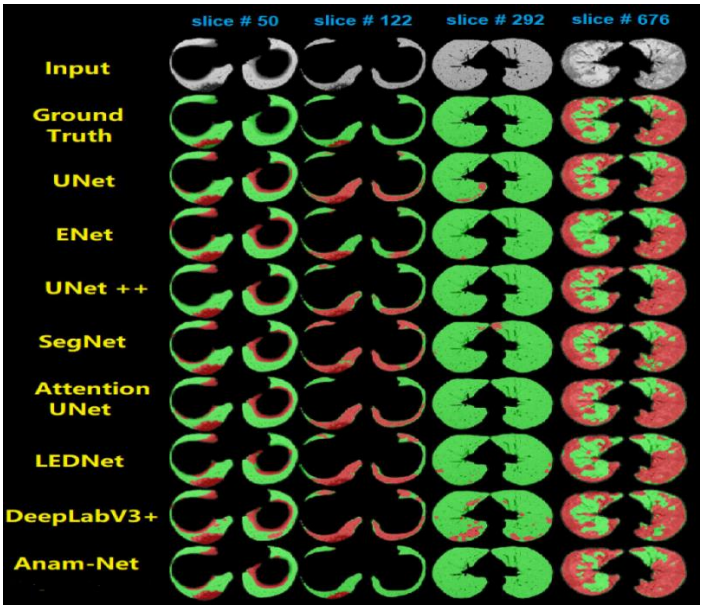

Figure 3 shows the representative segmentation results of the Experiment. The top row displayed slices of input (test cases) that were randomly chosen. The second row displays the annotations (ground truth). The normal lung area is shown in green, and the lung area with anomalies is shown in red. Table VI displays the aberrant lung areas' dice similarity ratings for these test instances.

In terms of sensitivity, accuracy, specificity, and Dice score, the proposed Anam-Net performed better than expected. UNet++ also performed well due to its hierarchical encoder-decoder design with extensive dense connections.

Overall, Anam-Net outperformed other networks with its lightweight design and anamorphic depth embeddings. Despite containing just 4.47 million (third fewest) parameters surpassed other models in all figures of merit. Heavy networks like Table V presented the averaged results from Experiment 1, while Tables VI showed results DeepLabV3+ (Experiment 3), with results that were comparable to those of Attention UNet.performed quite well

even in the cross-data set had an inferior performance.

TABLE IV Scores On A Dice Comparison For The Abnormal Lung Region Average Results Are Represented By The Last Row For The Test Case Listed. The Best Results Were In Bold.

Model Slice No.	UNet	Attention UNet	ENet	SegNet	UNet ++	DeepLab V3 +	LEDNet	**Anam -Net**
50	0.36	0.33	0.30	0.35	0.44	0.26	0.37	**0.38**
122	0.16	0.16	0.28	0.12	0.19	0.13	0.14	**0.80**
292	0.00	1.00	0.00	0.00	0.00	0.00	0.00	**1.00**
676	0.90	0.89	0.81	0.86	0.90	0.86	0.84	**0.89**
Average	0.36	0.60	0.35	0.33	0.39	0.31	0.34	**0.77**

TABLE V Contains The Averaged Merit Figures For Experiment 1 Used 704 Chest CT Images (Test Cases), And The Boldest Findings Were The Best

Model	Class	Dice Score	Specificity	Sensitivity	Accuracy
UNet	abnormal	0.608	0.983	0.932	0.982
	normal	0.943	0.997	0.902	0.981
SegNet	abnormal	0.587	0.981	0.936	0.980
	normal	0.935	0.995	0.897	0.978
Attention UNet	abnormal	0.695	0.988	0.951	0.987
	normal	0.960	0.997	0.932	0.986
DeepLabV3 +	abnormal	0.366	0.958	0.850	0.956
	normal	0.850	0.993	0.762	0.954
ENet	abnormal	0.694	0.990	0.857	0.988
	normal	0.956	0.991	0.954	0.985
UNet ++	abnormal	0.674	0.986	0.954	0.986
	normal	0.955	0.997	0.924	0.985
LEDNet	abnormal	0.597	0.983	0.907	0.981
	normal	0.929	0.991	0.901	0.976
	abnormal	**0.755**	**0.993**	**0.900**	**0.991**
Anam-Net	**normal**	**0.972**	**0.997**	**0.959**	**0.990**

from Experiment 2. The proposed Anam-Net, with fewer parameters, provided accurate segmentation compared to existing models. Anam-Net analysis

In conclusion, the proposed Anam-Net proved to be highly effective in segmenting COVID-19 anomalies,

TABLE VI Averaged The Merit Figures Over The 545 Chest CT Scans Included In Experiment 2 Are Test Cases Across Three Cross Folds. The Boldest Results Are The Best

Model	Class	Dice Score	Specificity	Sensitivity	Accuracy
UNet	Abnormal	0.791	0.990	0.907	0.988
	Normal	0.938	0.995	0.913	0.987
SegNet	Abnormal	0.612	0.988	0.657	0.980
	Normal	0.885	0.987	0.888	0.977
DeepLabV3 +	Abnormal	0.563	0.992	0.521	0.981
	Normal	0.895	0.983	0.930	0.978
ENet	Abnormal	0.686	0.989	0.736	0.984
	Normal	0.911	0.989	0.914	0.912
Attention UNet	Abnormal	0.783	0.987	0.966	0.987
	Normal	0.930	0.997	0.884	0.986
LEDNet	Abnormal	0.707	0.989	0.782	0.984
	Normal	0.899	0.987	0.912	0.979
UNet ++	Abnormal	0.805	0.990	0.951	0.988
	Normal	0.937	0.995	0.906	0.987
	Abnormal	**0.798**	**0.990**	**0.918**	**0.988**
Anam -Net	**Normal**	**0.941**	**0.997**	**0.911**	**0.988**

making it suitable for effective in segmenting COVID-19 anomalies, making it suitable for point-of-care platforms, while maintaining accuracy and quick inference.

]VI. CONCLUSION

In conclusion, this research introduced Anam-Net, a lightweight CNN based on anamorphic depth embeddings, designed to identify anomalies in chest CT scans using COVID-19. Given the significance of chest CT imaging in COVID-19 continues to increase management, this methodology is highly relevant.

The results from the three experiments demonstrated that Anam-Net achieved favorable scores on the dice for similarity to both abnormal and normal regions in chest CT images. Additionally, when compared to state-of-the-art lightweight and heavy networks like UNet, LEDNet, ENet, Attention UNet, UNet++, SegNet, DeepLabV3+, Anam-Net outperformed in terms of specificity, accuracy, and Dice score across all experiments.

Anam-Net's key advantage lies in its low computational complexity, requiring only 50% of the training time compared to the next best-performing network and having seven times fewer parameters. This makes it well-suited for deployment in clinical settings. The model size, being 17.2 MB, allows easy deployment on mobile platforms, facilitating rapid evaluation of anomalies in chest CT images from COVID-19.

In real-world deployment on hardware platforms for mobile and embedded, Anam-Net has proven to be highly suitable for point-of-care settings. Its effectiveness and efficiency make it a valuable tool for healthcare practitioners in managing COVID-19 cases according to chest CT imaging.

REFERENCES

1. C. Wang, P. W. Horby, F. G. Hayden, and G. F. Gao, “A novel coronavirus outbreak of global health concern,” Lancet, vol. 395, no. 10223, pp. 470–473, Feb. 2020.
2. C. Huang et al., “Clinical features of patients infected with 2019 novel coronavirus in Wuhan, China,” Lancet, vol. 395, no. 10223, pp. 497–506, Feb. 2020.
3. T. Ai et al., “Correlation of chest CT and RT-PCR testing in coronavirus disease 2019 (COVID-19) in China: A report of 1014 cases,” Radiology, vol. 2019, Feb. 2020, Art. no. 200642.
4. F. Shi et al., “Review of artificial intelligence techniques in imaging data acquisition, segmentation and diagnosis for COVID-19,” IEEE Rev. Biomed. Eng., early access, Apr. 16, 2020, doi: 10.1109/RBME.2020.2987975.
5. Y. Fang et al., “Sensitivity of chest CT for COVID-19: Comparison to RT-PCR,” Radiology, Feb. 2020, Art. no. 200432, doi: 10.1148/radiol.2020200432.
6. M.-Y. Ng et al., “Imaging profile of the COVID-19 infection: Radiologic findings and literature review,” Radiol., Cardiothoracic Imag., vol. 2, no. 1, Feb. 2020, Art. no. e200034.
7. COVID-19 CT Segmentation Dataset. Accessed: Apr. 11, 2020. [Online]. Available: https://medicalsegmentation.com/covid19/
8. Z. Ye, Y. Zhang, Y. Wang, Z. Huang, and B. Song, “Chest CT manifestations of new coronavirus disease 2019 (COVID-19): A pictorial review,” Eur. Radiol., pp. 1–9, Mar. 2020, doi: 10.1007/s00330-020- 06801-0.
9. J. P. Cohen, P. Morrison, and L. Dao, “COVID-19 image data collection,” 2020, arXiv:2003.11597. [Online]. Available: http://arxiv. org/abs/2003.11597
10. V. Rajinikanth, N. Dey, A. N. J. Raj, A. E. Hassanien, K. C. Santosh, and N. S. M. Raja, “Harmony-search and otsu based system for coronavirus disease (COVID-19) detection using lung CT scan images,” 2020, arXiv:2004.03431. [Online]. Available: http://arxiv.org/abs/ 2004.03431
11. L. Wang and A. Wong, “COVID-Net: A tailored deep convolutional neural network design for detection of COVID-19 cases from chest radiography images,” Mar. 2020, arXiv:2003.09871. [Online]. Available: https://arxiv.org/abs/2003.09871
12. J. Zhang, Y. Xie, Y. Li, C. Shen, and Y. Xia, “COVID-19 screening on chest X-ray images using deep learning based anomaly detection,” 2020, arXiv:2003.12338. [Online]. Available: http://arxiv. org/abs/2003.12338
13. X. Xu et al., “Deep learning system to screen coronavirus disease 2019 pneumonia,” 2020, arXiv:2002.09334. [Online]. Available: http://arxiv. org/abs/2002.09334
14. C. Zheng et al., “Deep learning-based detection for COVID-19 from chest CT using weak label,” MedRxiv, Mar. 2020, doi: 10.1101/2020.03.12.20027185.
15. S. Chaganti et al., “Quantification of tomographic patterns associated with COVID-19 from chest CT,” 2020, arXiv:2004.01279. [Online]. Available: http://arxiv.org/abs/2004.01279
16. F. Shan et al., “Lung infection quantification of COVID-19 in CT images with deep learning,” 2020, arXiv:2003.04655. [Online]. Available: http://arxiv.org/abs/2003.04655
17. A. Paszke, A. Chaurasia, S. Kim, and E. Culurciello, “ENet: A deep neural network architecture for real-time semantic

segmentation," 2016, arXiv:1606.02147. [Online]. Available: http://arxiv.org/abs/1606.02147

18. O. Ronneberger, P. Fischer, and T. Brox, "U-Net: Convolutional networks for biomedical image segmentation," in Medical Image Computing and Computer-Assisted Intervention (MICCAI) (Lecture Notes in Computer Science), vol. 9351. Cham, Switzerland: Springer, 2015, pp. 234–241. [Online]. Available: https://arxiv.org/abs/1505.04597 and [Online]. Available: http://lmb.informatik.uni-freiburg.de/Publications/2015/RFB15a
19. Z. Zhou, M. M. R. Siddiquee, N. Tajbakhsh, and J. Liang, "UNet++: Redesigning skip connections to exploit multiscale features in image segmentation," IEEE Trans. Med. Imag., vol. 39, no. 6, pp. 1856–1867, Jun. 2020.
20. V. Badrinarayanan, A. Kendall, and R. Cipolla, "SegNet: A deep convolutional encoder-decoder architecture for image segmentation," IEEE Trans. Pattern Anal. Mach. Intell., vol. 39, no. 12, pp. 2481–2495, Dec. 2017.
21. O. Oktay et al., "Attention U-net: Learning where to look for the pancreas," 2018, arXiv:1804.03999. [Online]. Available: http://arxiv.org/abs/1804.03999
22. Y. Wang et al., "Lednet: A lightweight encoder-decoder network for realtime semantic segmentation," in Proc. IEEE Int. Conf. Image Process. (ICIP), Sep. 2019, pp. 1860–1864.
23. L.-C. Chen, Y. Zhu, G. Papandreou, F. Schroff, and H. Adam, "Encoderdecoder with atrous separable convolution for semantic image segmentation," in Proc. Eur. Conf. Comput. Vis. (ECCV), 2018, pp. 801–818.
24. J. Hofmanninger, F. Prayer, J. Pan, S. Rohrich, H. Prosch, and G. Langs, "Automatic lung segmentation in routine imaging is primarily a data diversity problem, not a methodology problem," 2020, arXiv:2001.11767. [Online]. Available: http://arxiv.org/abs/2001.11767 .
25. K. He, X. Zhang, S. Ren, and J. Sun, "Deep residual learning for image recognition," in Proc. IEEE Conf. Comput. Vis. Pattern Recognit. (CVPR), Jun. 2016, pp. 770–778.
26. C. Szegedy et al., "Going deeper with convolutions," in Proc. IEEE Conf. Comput. Vis. Pattern Recognit. (CVPR), Jun. 2015, pp. 1–9.
27. S. Ioffe and C. Szegedy, "Batch normalization: Accelerating deep network training by reducing internal covariate shift," 2015, arXiv:1502.03167. [Online]. Available: http://arxiv.org/abs/1502.03167
28. A. Krizhevsky, I. Sutskever, and G. E. Hinton, "Imagenet classification with deep convolutional neural networks," in Proc. Adv. Neural Inf. Process. Syst., 2012, pp. 1097–1105.
29. COVID-19 Database. Accessed: May 29, 2020. [Online]. Available: https://www.sirm.org/en/category/ articles/covid-19-database/
30. COVID-19. Accessed: May 29, 2020. [Online]. Available: https://radiopaedia.org/articles/covid-19-3
31. A. Paszke et al., "Pytorch: An imperative style, high-performance deep learning library," in Proc. Adv. Neural Inf. Process. Syst., 2019, pp. 8026–8037.
32. D. P. Kingma and J. Ba, "Adam: A method for stochastic optimization," 2014, arXiv:1412.6980. [Online]. Available: http://arxiv.org/abs/1412.6980
33. S. Ioffe and C. Szegedy, "Batch normalization: Accelerating deep network training by reducing internal covariate shift," 2015, arXiv:1502.03167. [Online]. Available: http://arxiv.org/abs/1502.03167